photonics

MDPI

Article

Development of Miniaturised Fibre-Optic Laser Doppler Velocimetry for Opaque Liquid: Measurement of the Velocity Profile in the Engine Oil Flow of a Lubrication System

Tsutomu Tajikawa [1,*], Shimpei Kohri [2], Taiki Mouri [3], Takaichi Fujimi [3], Hiromasa Yamaguchi [3] and Kenkichi Ohba [4,†]

[1] Department of Mechanical Engineering, Faculty of Engineering Science, Kansai University, Osaka 564-8680, Japan
[2] Department of Medical Engineering, Faculty of Health Sciences, Aino University, Osaka 567-0012, Japan; s-kohri@me-u.aino.ac.jp
[3] Graduate School of Science and Engineering, Kansai University, Osaka 564-8680, Japan
[4] Faculty of Engineering, Kansai University, Osaka 564-8680, Japan; ohba4202@kjc.biglobe.ne.jp
* Correspondence: tajikawa@kansai-u.ac.jp; Tel.: +81-6-6368-3047
† Emeritus Professor.

Abstract: This study developed a fibre-optic laser Doppler velocimetry sensor for use in opaque, high-temperature, and high-pressure fluid flows by inserting the fibre perpendicular to the main flow. The tip of the optical fibre was obliquely polished and chemically etched using a buffered hydrofluoric acid solution, and a reflective mirror was deposited on the surface of the oblique fibre tip. Based on the results of the verification test using the rotating annular open channel, the fabrication conditions of the fibre tip were optimized for measuring the lubricating oil flow. The flow velocity profiles in the engine's oil flow of the lubrication system during engine bench testing were measured. These velocity profiles were influenced by variations in the measurement position, oil temperature, and engine speed. The measurement accuracy of this sensor was compared with the volumetric flow rate obtained by cross-sectional area integration of the flow velocity profile, as measured using a Coriolis flowmeter, and the difference was within 1%. By combining computational simulation for flow and optical attenuation and particle scattering in light transmission through a working fluid, this fibre-optic sensor achieved a measurement volume of 200 microns in length and 200 microns in width at a distance of 900–1000 microns from the sensor.

Keywords: laser Doppler velocimetry; fibre-optic sensor; lubricant oil; opaque liquid flow velocity measurement; high-pressure; high-temperature flow

Citation: Tajikawa, T.; Kohri, S.; Mouri, T.; Fujimi, T.; Yamaguchi, H.; Ohba, K. Development of Miniaturised Fibre-Optic Laser Doppler Velocimetry for Opaque Liquid: Measurement of the Velocity Profile in the Engine Oil Flow of a Lubrication System. *Photonics* **2024**, *11*, 892. https://doi.org/10.3390/photonics11090892

Received: 30 July 2024
Revised: 17 September 2024
Accepted: 19 September 2024
Published: 22 September 2024

1. Introduction

Laser Doppler velocimetry (LDV) is a well-known flow velocity measurement method that utilises the wavelength of a laser as a gauge, thus allowing for absolute measurement without the need for calibration. In particular, LDV is characterised by a high measurement accuracy, a small measurement volume, and high time resolution. It can be used to measure flows across a broad spectrum of velocities from low to high, including those with large velocity gradients such as boundary layers. This versatility has significantly advanced the fields of fluid mechanics and fluid engineering. However, LDV cannot be used to measure flow velocities in fluids that are opaque to lasers. Moreover, even in transparent fluids, it is necessary to install an observation window in the tube wall to allow for the passage of light, which can lead to issues in high-temperature and high-pressure environments.

To address these limitations, Tanaka and Benedek [1] and Kajiya et al. [2–7] developed fibre-optic LDV (FO-LDV) sensors capable of measuring the velocity of blood flow in vivo. These sensors involved the insertion of optical fibres through a needle or catheter introduced

into a blood vessel. The laser emitted from the optical fibre tip was scattered by erythrocytes within the blood flow. The scattered laser light was collected by the same fibre, and the heterodyne interference created by superimposing the scattered laser and local oscillator light was then detected by a photomultiplier tube to measure the Doppler frequency, which correlated with the erythrocytes' velocity. In contrast to dual-beam LDV, where the measurement volume is defined and the flow velocity component in a specific direction can be precisely determined, the measurement volume of FO-LDV is less distinct, and the Doppler frequency represents the erythrocytes' approach speed towards the fibre tip. Additionally, the frequency spectrum of the interference light generally does not exhibit a clear peak, with a broad peak overlapping the pedestal noise, complicating the identification of the Doppler frequency. To address these issues, we previously attached a gradient-index lens to the fibre tip [8] and chemically etched the fibre tip to create a convex lens shape [9], thereby focusing the emitted laser beam. By positioning the chemically etched fibre tip at an angle to the blood flow, we successfully measured the velocity profiles of the entire blood flow and the time-resolved unsteady flow velocity [10]. However, with an increase in the fibre's insertion angle relative to the vessel wall, the measurement error increased. To enhance the measurement accuracy, it is essential to align the direction of laser emission from the fibre tip parallel to the flow [10–12].

With reference to the available literature, the velocity profiles of the lubricating oil flow in an automotive engine, which represents a more optically challenging environment than blood flow, have not been previously measured. Thus, we developed an FO-LDV sensor with the fibre sensor inserted perpendicularly to the tube wall. We applied this fibre sensor to measure the local flow velocity of lubricating oil during testing an automobile engine. Additionally, we estimated the measurement volume for this sensor for the measurement of the flow velocity in lubricating oil by simulating the flow around the fibre tip, the transmission attenuation of the laser in lubricating oil, and the scattering by solid lubricants.

2. Materials and Methods

2.1. Design and Prototyping of a Normally Inserted FO-LDV Sensor for Velocity Measurements in Opaque Fluid

Figure 1a illustrates the design of the FO-LDV sensor and the method for accessing the flow channel. The optical fibre was attached perpendicularly to the flow channel's wall using a helicoidal gear-type traverser, which was engineered to measure the flow velocity profile in the channel. This traverser was designed to hold the optical fibre and a stiffening tube, which consisted of a stainless-steel tubing, thus protecting against excessive mechanical stress and facilitating the insertion and removal of the fibre into the channel without rotation. As depicted in Figure 1b, the tip of the optical fibre was cut at a 45° angle relative to the longitudinal axis of the fibre, and a reflector was formed on the tip's surface.

The optical fibre employed was a graded index (GI) multi-mode fibre (Sumitomo Electric, Osaka, Japan, GI(PE-A1G)-C, with a core diameter of 50 μm, a cladding diameter of 125 μm, and a numerical aperture of 0.21), which was selected for its high efficiency in receiving weakly scattered light. After cutting the bare fibre with an optical-fibre cutter, the protective coating layer was removed, and the fibre tip was polished. Figure 1c presents the optical fibre positioned obliquely at 45° against the surface of the polishing film on an optical fibre rotation/revolution polishing machine (Seiko Giken, Matsudo, Japan, SFP-70D2), where the tip was polished with a fibre-axial feed. To mitigate the deflection of the optical fibre during polishing, it was temporarily inserted into stainless-steel tubing, which was made from combinations of three different sizes of stainless-steel tubes (thinnest tube: inner diameter (ID), 150 μm; outer diameter (OD), 300 μm; middle tube: ID, 300 μm; OD, 550 μm; thickest tube: ID, 700 μm; OD, 1060 μm).

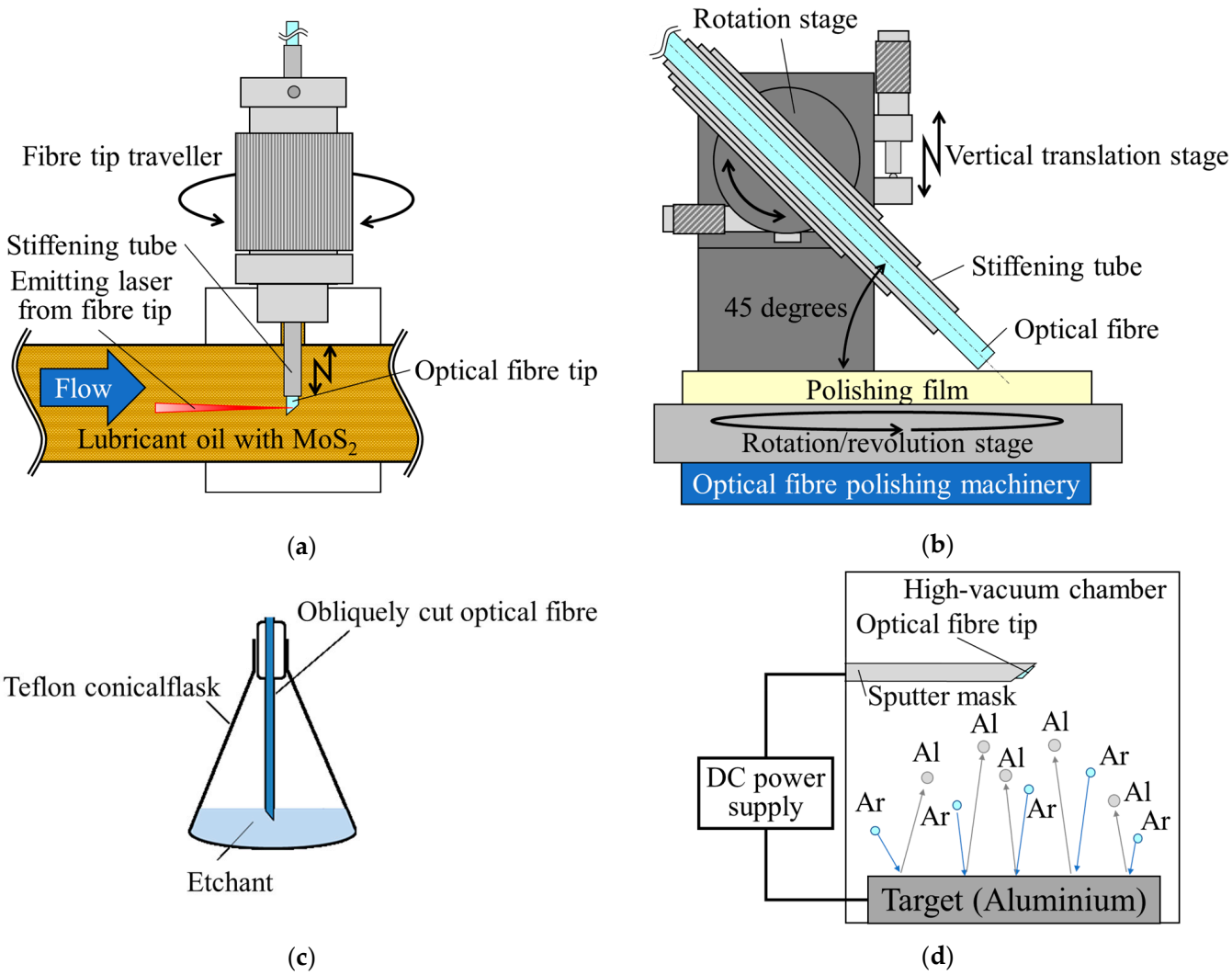

Figure 1. Design and fabrication processes for the normally inserted FO-LDV sensor. (**a**) Schematic of the FO-LDV sensor designed for normal insertion against the main flow and the fibre tip traverser for measuring the flow velocity profile. (**b**) Schematic of the oblique polishing process. The optical fibre and its holder for the stiffening of the fibre are shown in sectional views. (**c**) Schematic of the chemical etching process. (**d**) The process of forming the reflection mirror utilised direct current (DC) sputtering. By employing a mask tube, the aluminium mirror was formed on the surface of the fibre's end.

The tip-polishing process comprised three steps. Initially, rough polishing was performed for 5 min using a rough-polishing film (Seiko Giken, DR07-9U) with ultrapure water as the lubricant and a feed speed of 20 mm/min. Subsequently, normal finishing occurred for 2.5 min using a semi-polishing film (Seiko Giken, DH07-3U) with anhydrous ethanol as the lubricant and the same feed speed. Thereafter, mirror finishing was conducted for 2 min using a finishing film (Seiko Giken, SF07) with ultrapure water as the lubricant, without any feed. The rotation/revolution speeds of the polishing machinery remained unchanged from the original settings. After the polishing process, the fibre tip was rinsed in ultrapure water in an ultrasonic bath for 5 min and then air-dried before proceeding to the following step.

The surface of the optical fibre tip was chemically etched to form a convex surface. Previous research demonstrated that a convex lens-shaped fibre tip was produced when a quartz GI optical fibre was immersed in a buffered hydrofluoric acid etchant composed of 50% wt hydrogen fluoride (HF, Daikin Chemicals, Osaka, Japan) and 40% wt ammonium fluoride (NH_4F, Daikin Chemicals) diluted in pure water (H_2O), as shown in Figure 1c [9,10]. This technique allowed for the adjustment of the convex/concave shape and the curvature of the lens by controlling the concentration ratio of the etchant and the duration of the etching process. In this study, the curvature of the convex surface on the fibre tip was adjusted by managing the etching time with a volumetric concentration ratio of $HF:NH_4F:H_2O$ = 1:7:2.5 at an etching temperature of 25 °C [9,10].

As the final step in fabricating the FO-LDV sensor, a metal film was deposited on the end of the optical fibre with a convex surface to create an optical mirror. Preliminary studies indicated that aluminium films could be effectively coated using the DC sputtering technique. As depicted in Figure 1d, an optical fibre with a convex-shaped tip inclined at an angle of 45° was inserted into stainless-steel tubing (ID: 150 μm, OD: 300 μm) and placed within the vacuum chamber of a DC sputtering apparatus (Shibaura Mechatronics, CFS-8EP). The optical fibre and the stainless-steel tubing were precisely aligned such that only the convex-shaped tip of the optical fibre received the sputter-deposited metal film. Argon was used as the sputtering gas, with the other deposition conditions including a pressure of approximately 2×10^{-3} Torr, a voltage of 430 V applied to the target, and a current of 0.6 A. After sputtering for 30 min under these conditions, an aluminium film with an approximate thickness of 0.33 μm was deposited.

The FO-LDV sensor was finalized by attaching an FC connector to the opposite end of the optical fibre, inserting the sensor's tip into stiffening tubes composed of three different tubes (the thinnest tube had an ID of 150 μm and OD of 300 μm, the middle tube had an ID of 300 μm and an OD of 550 μm, and the thickest tube had an ID of 700 μm and an OD of 1060 μm), and securing the fibre within these tubes using heat-resistant glue (Toagosei, Tokyo, Japan, Aron Alpha EXTRA4000).

2.2. Verification of the Prototyped Fibre-Optic LDV Sensor in Lubricating Oil Flow

The measurement of flow velocity in opaque lubricant oil using the prototype FO-LDV sensor was conducted and evaluated. Figure 2a presents the configuration of the flow system with the schematics of the optical system and the signal processing system of the FO-LDV. In this experiment, a constant flow speed was achieved by rotating an annular open channel filled with engine oil at a constant rotational speed [9]. The engine oil contained in the rotating annular open channel underwent rigid rotation, referred to as a forced vortex in fluid mechanics. Consequently, the rotational velocity of the oil was proportional to both the radius and the angular velocity. When the FO-LDV sensor was inserted into the rotating oil, it measured the velocity proportional to the radius at which it was placed. The open annular channel used in this study was made of plexiglass, with an inner wall radius of 60 mm, an outer wall radius of 80 mm, and a depth of 40 mm. The FO-LDV sensor was positioned 76 mm from the centre of rotation of the annular channel, and the rotational speed was set at 26.5 rpm. Thus, the flow velocity was determined by multiplying the distance between the sensor's position and the rotational centre of the open channel by the rotational speed.

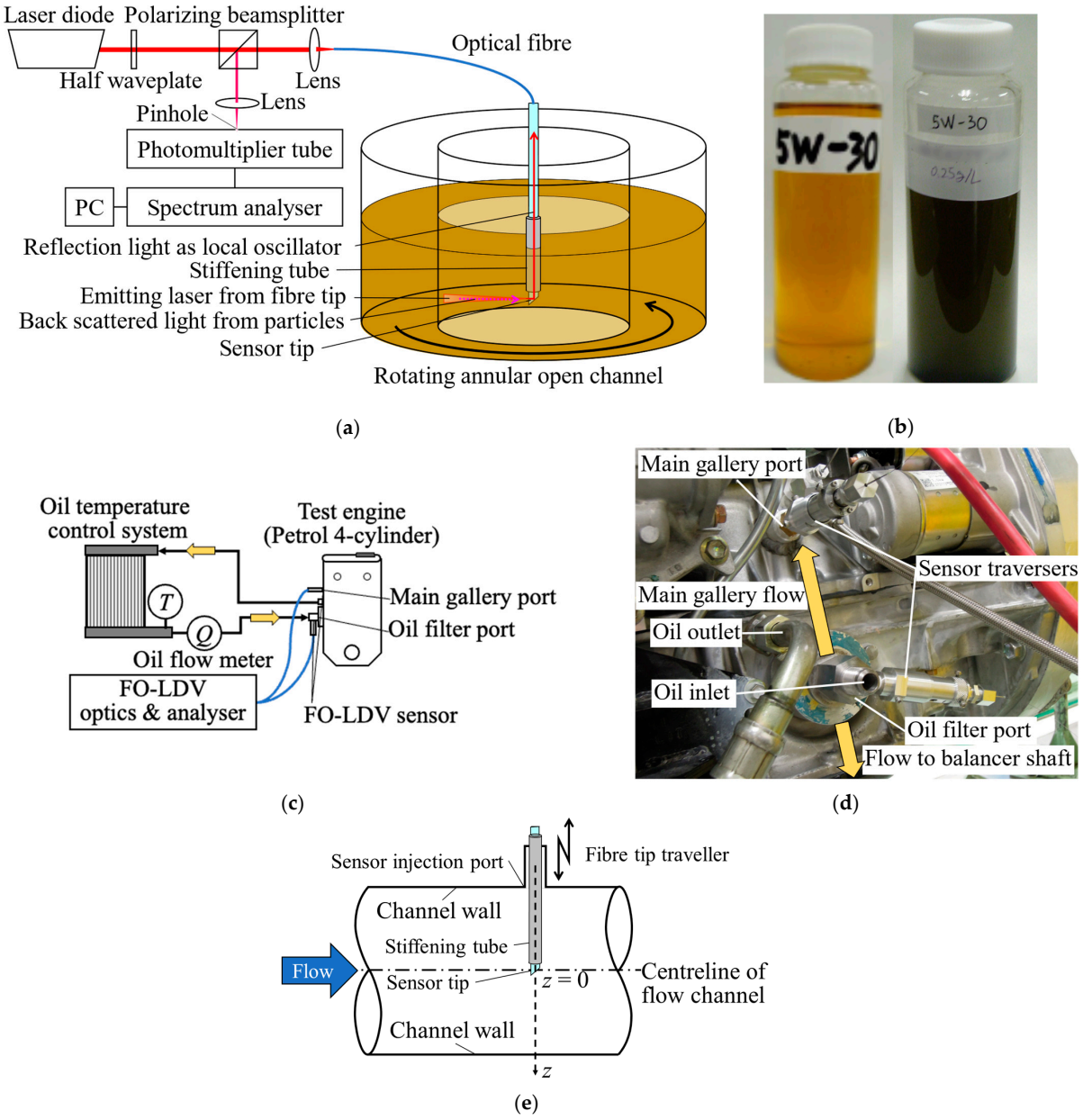

Figure 2. Outline of the verification and validation testing for the prototyped FO-LDV sensor. (**a**) Validation test setup using a rotating annular open channel and the optical system. By rotating the channel filled with the working fluid at a constant speed of revolution, a uniform flow velocity was generated, as calculated from both the rotating radius and the speed of revolution. (**b**) Examples of working fluids: unused lubricating oil (left) and deteriorated oil with MoS_2 powder after engine bench testing. (**c**) Overview of the lubricating flow system of the engine bench test and the verification test for the FO-LDV. (**d**) Measurement location of flow during the engine bench test. (**e**) The definition of the coordinate system for measurement of the velocity profile.

This optical system incorporated a reference beam. A monochromatic beam from a laser diode (CrystaLaser, Reno, NV, USA, DL640-038-3O; wavelength, λ_0 = 643 nm; power, 27 mW; beam diameter, 1.5 mm; beam divergence, 1 mrad) was polarised in parallel (P-polarised) after passing through a half-wave plate (Sigmakoki, Hidaka, Japan, WPM-10-2P). It was then transmitted by a polarising beam splitter (PBS, Sigmakoki, PBSW-10-550) and focused by a lens (Neoark, Hachioji, Japan, FIN-M50H) onto the tip of the optical fibre. The laser beam, after travelling through the optical fibre, was reflected by the concave

mirror at the fibre's end and transmitted from the sidewall of the fibre's end into the fluid. The longitudinal axis of the optical fibre was aligned perpendicular to the rotating plane, and the direction of the laser's path was parallel to the velocity of the rotating annular open channel. When scattering particles, such as air bubbles and solid lubricant particles, traversed the beam's path in the working fluid, they scattered the incident light and altered its frequency by the Doppler effect. Backscattered light was collected by the same fibre, whereas scattered light and light partially reflected at the fibre's end, which functioned as a local oscillator, were reflected by the PBS. The superimposed scattered light and the local oscillator's light created heterodyne interference, as detected by a photomultiplier tube (Hamamatsu Photonics, Hamamatsu, Japan, R1477-06). The Doppler signal, which was detected via heterodyne interferometry, was processed by a swept-tuned spectrum analyser (SA, Advantest, Tokyo, Japan, TR4170) over a 120-s sweep time frequency spectrum and recorded by a personal computer (PC). The peak in each spectrum was identified as the Doppler frequency f_D. The relationship between the Doppler frequency and the flow velocity can be expressed as Equation (1)

$$f_D = \frac{2n}{\lambda_0}|u\cos\theta|, \tag{1}$$

where n is the refractive index of the working fluid and θ is the angle between the direction of the laser beam's emission and the flow velocity u. Given that $\theta = 0^\circ$ in this optical setup, Equation (1) simplifies to Equation (2):

$$f_D = \frac{2n}{\lambda_0}|u|. \tag{2}$$

The frequency spectrum of the Doppler signal thus represented the probability density function of the flow velocity over 120 s. The measured flow velocity, as derived from the detected Doppler frequency in the spectrum, indicated the time-averaged flow velocity across this 120 s period.

To simulate the lubricating oil flow, automobile engine oil (5W-30, dynamic viscosity μ = 82.1 mPa·s; refractive index n = 1.466 at 25 °C) was used at room temperature, supplemented with molybdenum disulphide (MoS_2) powder (Daizo Corp., Nichimoly Div., Osaka, Japan, M-5; median particle diameter, 1.69 μm; density, 4800–5000 kg/m^3) as a solid lubricant and as tracer particles for LDV at a concentration (C) of 0.25 g/L, as shown in Figure 2b.

2.3. Measurement of the Velocity Profile in the Lubricating Oil Flow during Testing the Automobile Engine

To verify the effectiveness of the FO-LDV sensor developed in this study, measurements of the velocity profiles in a lubricating oil flow during an engine test were conducted. As shown in Figure 2c, an automotive four-stroke, four-cylinder petrol engine was operated on an engine bench. The lubricating oil's temperature was maintained at 80 °C using an externally installed oil cooler, and a Coriolis flow meter (Keyence, Osaka, Japan FD-SS20A) was connected in the tubing between the engine and the oil cooler to monitor the flow rate. As shown in Figure 2d, the FO-LDV sensor was mounted at two locations: one at the oil line's connection port, where the engine's oil filter is typically installed (hereafter referred to as the oil filter location), and the other at the oil's main gallery in the engine cylinder block downstream of the oil filter (hereafter referred to as the main gallery location). The fibre-optic sensor was attached to the engine via a custom-made helicoidal traverser, thus allowing for the position of the fibre tip in the oil line to be adjusted without rotating the fibre. As shown in Figure 2e, the velocity profiles in the lubricating oil flow were measured by moving the FO-LDV sensor's tip along the z-axis, which was defined as the direction of the longitudinal axis of the optical fibre. The origin of the z-axis was set at the centre of the lubricating oil's channel. In the experiment, molybdenum disulphide powder was added to 5W-30 engine oil at a concentration of C = 0.25 g/L. The properties of the engine oil at a

temperature of 80 °C were as follows: refractive index n = 1.447; density ρ = 813.1 kg/m^3; dynamic viscosity μ = 8.76 m·Pa·s; kinematic viscosity ν = 10.7 mm^2/s. The engine bench test included two 2 h warm-up sessions using fresh engine oil. During the engine bench test, the engine speed was regulated by the engine bench system, with the engine operating at constant speeds (N) of 2000 rpm, 3000 rpm, 4000 rpm, 5000 rpm, and 6000 rpm during the flow velocity measurements. At each operating condition and location of the sensor, the fibre tip was moved in increments of 1 mm to measure the velocity profiles in the oil gallery with an inner diameter of 14 mm.

3. Results

The results obtained in this study are presented in this section in accordance with the sequence described in the Materials and Methods section.

3.1. Design and Prototype of the FO-LDV Sensor

Examples of both an optical micrograph and an electron micrograph of an optical fibre with the tip polished at an angle of 45° are shown in Figure 3a. The end surface of the optical fibre was polished sufficiently, with no visible scratches. The angle between the polished surface and the optical fibre's axis for 33 fabricated samples was measured from the optical microscopy images. As shown in Figure 3b, the mean angle of the fabricated tip was 45.9°, with a standard deviation of ±1.4°. The cause of this fabrication error can be attributed to the flexure of the stainless-steel tubing used to hold the optical fibre when the fibre tip was pressed against the polisher. However, according to Equation (1), even if an error of $\theta = \pm 5°$ occurred, the maximum measurement error caused by this fabrication error would be considerably small, i.e., 0.5%, in the configuration of the optical system of this FO-LDV sensor. Hence, the influence of the accuracy of fabrication on the measurement was considered negligible.

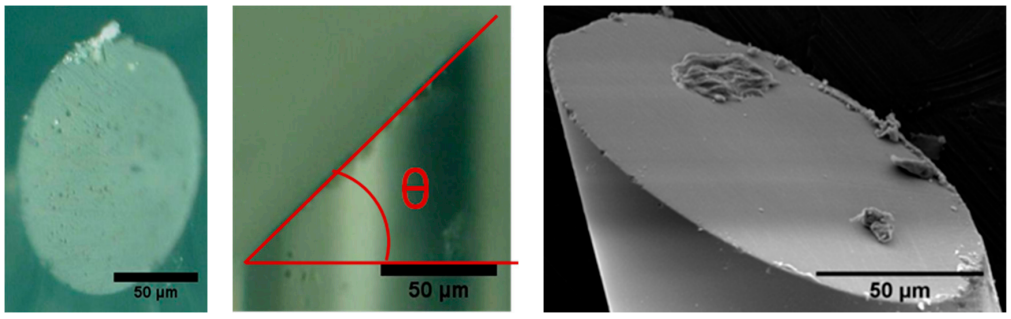

Polished surface Side view Scanning electron microscopy image

(**a**)

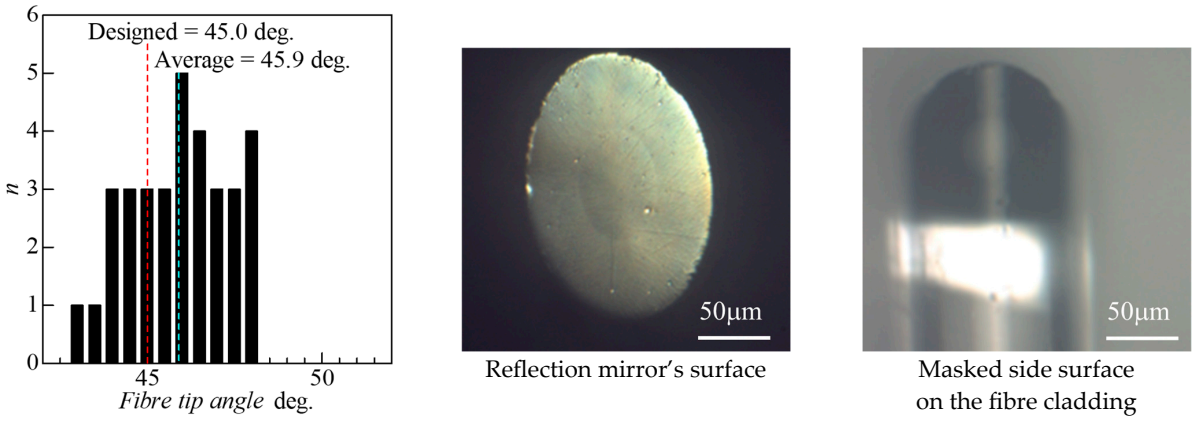

(**b**) Reflection mirror's surface Masked side surface on the fibre cladding

(**c**)

Figure 3. *Cont.*

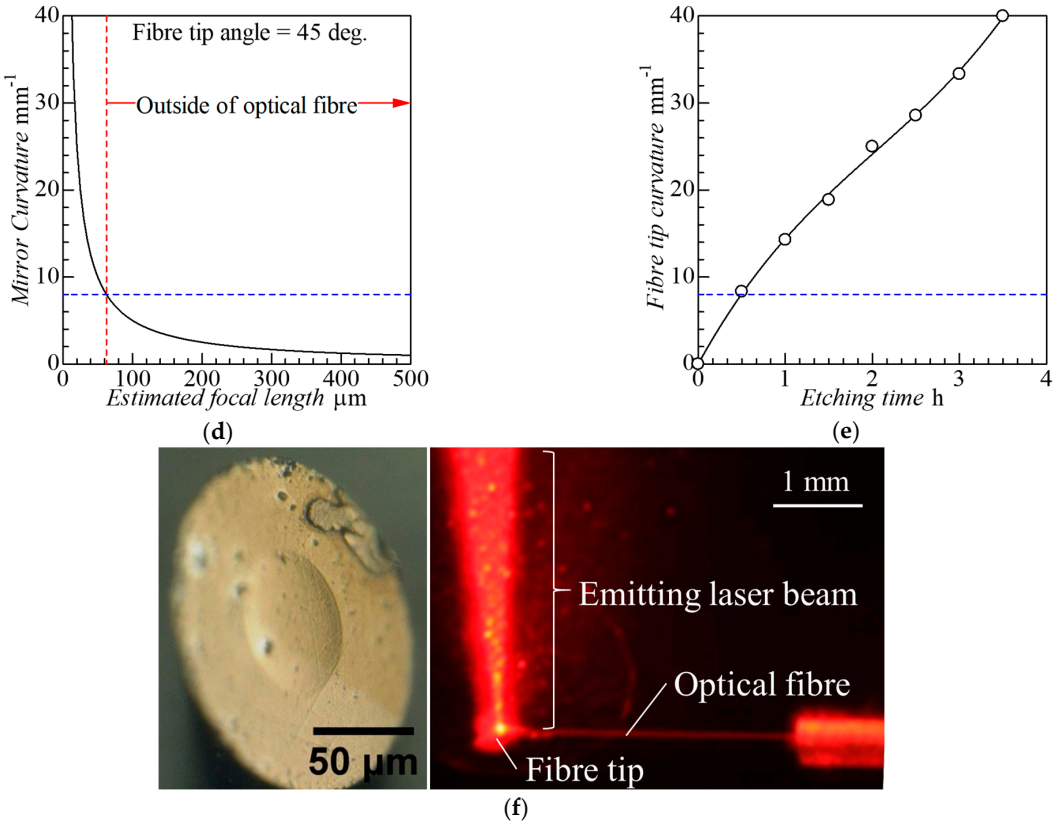

Figure 3. Results of FO-LDV prototyping. (**a**) Examples of the obliquely cut fibre tip. Optical micrograph of the polished surface (left). Side view of the obliquely cut fibre tip (middle). Scanning electron micrograph of the polished fibre tip, which was coated by platinum (right), with debris caused by inadequate cleaning. (**b**) Histogram of the angle of the polished surface of the optical fibres. (**c**) Example of the reflection mirror deposited on the optical fibre tip. Optical micrograph of the mirror's surface without the etching process (left). By masking the optical fibre, a reflection mirror did not form on the sidewall (right). (**d**) Result of simulating the relationship between the reflection mirror's curvature and the focal length of the superimposed path of the laser from the fibre. (**e**) Relationship between the chemical etching time and the curvature of the surface of the chemically etched optical fibre tip. The plots indicate the experimental results, and the rigid line indicates a cubic function as an approximation of the experimental result. (**f**) Example of a fabricated FO-LDV sensor. Optical micrograph of the FO-LDV with a curved surface on the tip (left). The laser beam was emitted from the fibre's sidewall after being reflected at the obliquely placed curved mirror (right). The laser's path was visualised by the scattered particles in the fluid.

As an example of the results, an optical microscopy image of the fibre tip before and after immersion is shown in Figure 3c. Due to the convex surface formed on the end face of the optical fibre cut at an angle of 45° by chemical etching, the light emitted from the sidewall of the optical fibre was expected to be focused by reflection on its spherical surface. However, it should be noted that if the curvature of the spherical surface was considerably larger, a focus would be formed inside the fibre; thus, it was necessary to fabricate a curved mirror with an appropriate curvature. To design an appropriate curvature for the concave mirror, the optical path of the light reflected by the mirror at the fibre's end was simulated using ray optics theory. This simulation considered the distribution of the refractive index in the fibre's core, assuming that the laser propagated uniformly as collimated light within the fibre's core [9]. As depicted in Figure 3d, the results of simulating the optical path indicated that a focus was formed outside of the fibre when the curvature of the concave mirror was less than 8.0 mm^{-1}, at a distance of about 200 µm away from the fibre's sidewall when the curvature was 2.0 mm^{-1}, and at a distance of about 440 µm when the curvature

was 1.0 mm^{-1}. Therefore, we investigated the relationship between the etching time and the curvature of the optical fibre's surface obtained by chemical etching. As shown in Figure 3e, the curvature of the surface of the end of the optical fibre formed by etching at the fibre's core increased with an increase in the etching time. By approximating the relationship between the curvature and the etching time with a power function, it was demonstrated that the etching time was within about 30 min for the realization of a focus outside the optical fibre.

A sample was fabricated by chemically etching the tip of an optical fibre for a duration of 15 min, followed by the deposition of a reflective layer of aluminium on the optical fibre using DC sputtering to create a concave mirror. A laser was directed onto this fibre sample, and the laser light emitted from the fibre was observed under an optical microscope, as shown in Figure 3f. This result indicated that the laser was emitted from the sidewall of the fibre with minimal light leakage from the mirror. Although a focal point was expected to form at a distance of approximately 3.4 mm from the fibre's sidewall, the laser's path did not exhibit a clear focal point. This discrepancy can be attributed to the assumption that the laser propagating in the fibre's core was perfectly collimated in the simulation of the optical path. However, the laser beam emitted from the fibre had a narrower divergence angle when compared with the aperture of the bare optical fibre; hence, this optical fibre tip was employed as the FO-LDV sensor.

3.2. Verification of the Flow Measurement Performance of the Prototyped FO-LDV Sensor

An LDV system employing the prototype FO-LDV sensors was assembled and verified to measure the flow velocity in an engine's oil flow, which was generated by a rotating annular open channel with a known velocity. In this experiment, FO-LDV sensors were fabricated with chemical etching times of 1 min, 5 min, 7.5 min, 15 min, and 30 min. Consequently, the relationship between the curvature of the concave mirror fabricated on the fibre tip and the etching time was established using Figure 3e, as shown in Table 1. The radius of rotation and the rotational speed of the annular open channel were set at 73 mm and 26.5 rpm, respectively, equating to a rotational speed of 0.2025 m/s. The theoretical Doppler shift frequency calculated from Equation (2) was f_D = 923 kHz.

Table 1. Estimated relationship between the duration of chemical etching and the curvature of the fabricated curved mirror.

Etching time (min)	1.0	5.0	7.5	15	30
Estimated mirror curvature (mm^{-1})	0.3	1.5	2.2	4.3	8.1

Figure 4 illustrates the spectral waveform obtained from the spectral analyser for local velocity measurements performed using the FO-LDV sensor with different mirror curvatures. Several spectral peaks were observed at 0.5 MHz, 1.0 MHz, and 1.5 MHz. However, these peaks did not vary with changes in the rotational speed, thus indicating that they were noise originating from the laser diode. There was a signal with a broad frequency spectrum between the theoretical Doppler frequency and the pedestal noise component caused by the laser in each spectral waveform. This signal tended to broaden, and the signal's strength increased as the etching time decreased. Previous studies [9] indicated that flow velocity measurements using FO-LDV for opaque flows such as blood flow were realized when a steep change appeared on the spectral waveform and the steeply changing frequency was close to the actual Doppler frequency of the flow. Therefore, this result suggests that a fibre with an etching time of 1 min was the most appropriate for velocity measurements when applying the FO-LDV sensor for the measurement of a lubricant's flow velocity.

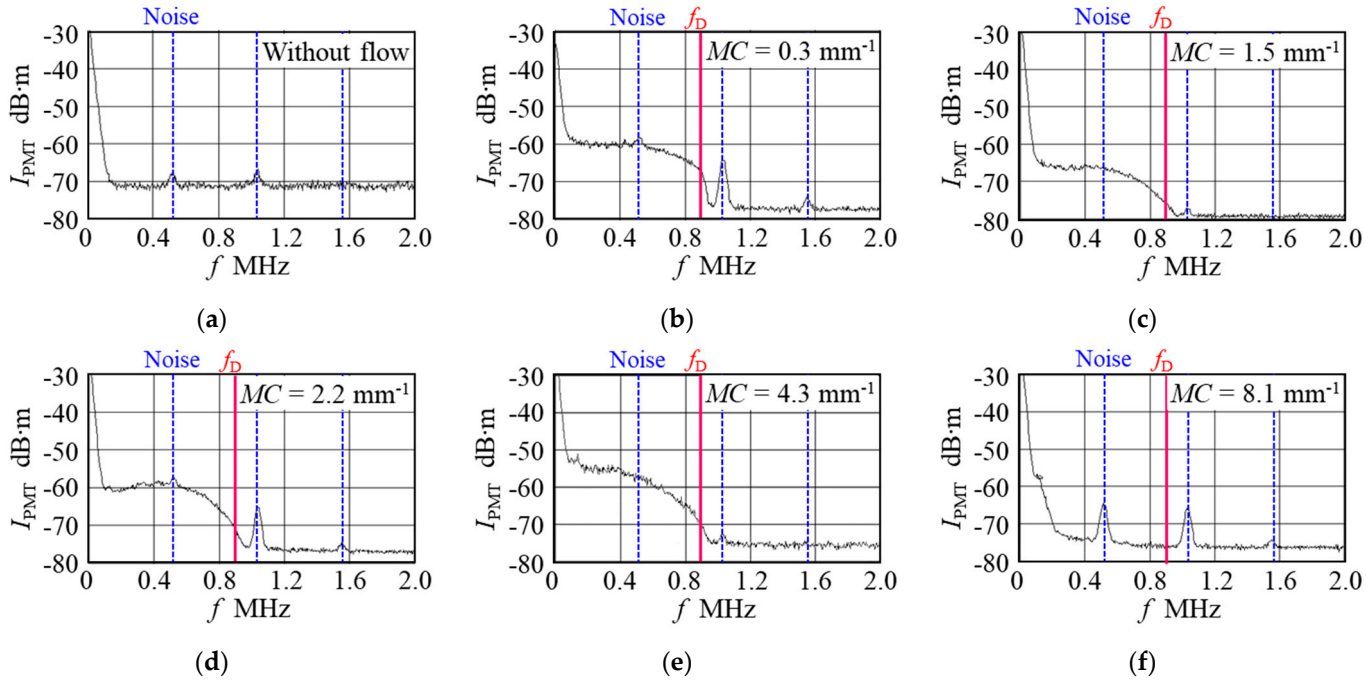

Figure 4. Examples of the spectral waveform of the validation test using a rotating annular open channel flow. (**a**) Typical spectral waveform without flow conditions, which exhibited pedestal noise and other noises (blue dashed lines). (**b**–**f**) Examples of spectral waveforms using the FO-LDV sensor with estimated mirror curvatures (*MC*) of (**b**) 0.3 mm^{-1}, (**c**) 1.5 mm^{-1}, (**d**) 2.2 mm^{-1}, (**e**) 4.3 mm^{-1}, and (**f**) 8.1 mm^{-1}. The red rigid line indicates the actual Doppler frequency (f_D) of the flow.

3.3. Validation of Local Flow Velocity Measurements in Lubricant Oil Flow during an Engine Bench Test

Figure 5a,b presents examples of the spectral waveforms obtained at both the oil filter's location and the main gallery of the engine's oil flow during the engine bench test [13]. These graphs illustrate the influence of engine speed and the position of the fibre tip within the cross-section of the flow channel on the spectral waveform. The engine oil was circulated by a gear pump connected to the engine's output shaft via a V-belt; thus, the flow rate was proportional to the engine speed. As the engine speed varied, the peak frequency of the spectral waveform tended to shift towards higher frequencies. The peak frequency shifted towards lower frequencies as the sensor's tip moved from the centre (z = 0 mm) of the cross-section of the gallery to a position near the gallery's wall (z = 6 mm) owing to the viscous effects of the oil. When the peak frequency in the spectral waveform dropped below about 0.5 MHz, the signals merged with the pedestal noise; thus, measurement became impossible.

In this study, the Doppler frequency was defined as the peak frequency on the spectral waveform. The flow velocity was calculated using the relationship expressed by Equation (2), and the relationship between the fibre tip's position in the oil gallery and the flow velocity was plotted. Figure 5c presents the velocity profile of the oil flow at both the oil filter port and the main gallery, while Figure 5d presents the velocity profiles of the main gallery. At the oil filter location, the flow velocity was measured only at an engine speed of 2000 rpm, with the maximum velocity in the cross-section located at a distance of 2–3 mm from the centre. After passing through the filter location, the oil flow was divided into two directions: into the main gallery in the cylinder block and towards the balancer shaft of the output shaft of the engine. The measured velocity profiles at the main gallery were almost axisymmetrical, thus indicating that the velocity profile was influenced by the bends in the tubing before and after the measurement location. This result suggested that the proposed FO-LDV sensor could accurately measure flow velocities in such complex flow fields.

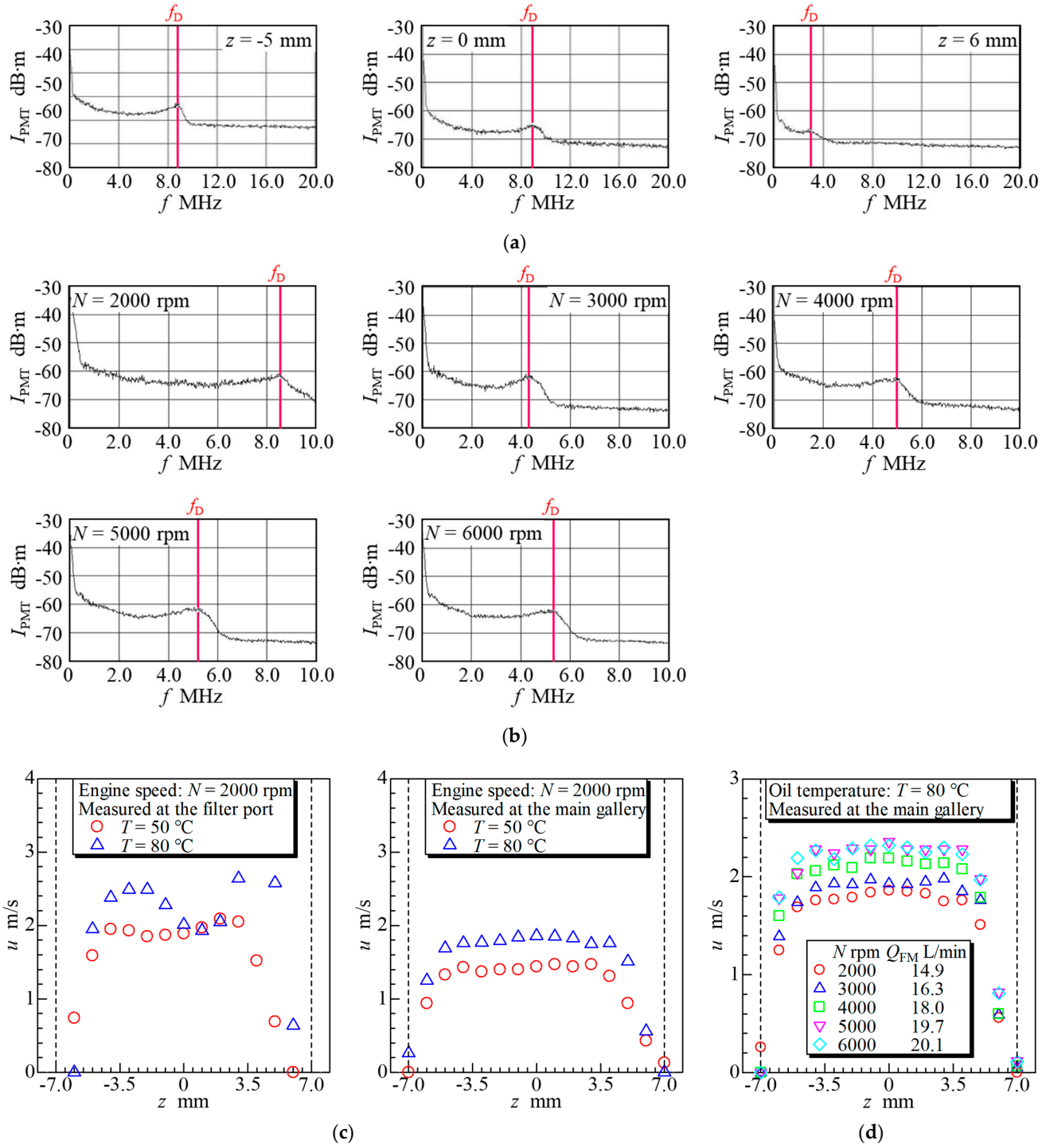

Figure 5. Examples from the verification test via the engine bench test. (**a**) Influence of different positions of the sensor in the cross-section of the oil gallery on the spectral waveforms as measured at the oil filter location under an engine speed N = 2000 rpm and an oil temperature T = 80 °C. The sensor's positions were z = −5 mm (left), z = 0 mm (middle), and z = 6 mm (right). (**b**) Influence of varying engine speeds on the spectral waveforms measured at z = 0 mm at the oil filter position and under T = 80 °C. (**c**) Measured velocity profiles during the engine bench test under N = 2000 rpm and T = 80 °C: results at the filter port (left) and main gallery (right), indicating that the flow profiles were influenced by the measurement location and the oil temperature. (**d**) Influence of engine speed on velocity profiles in the main gallery under constant oil temperature conditions.

4. Discussion

By obliquely cutting the tip of the optical fibre and forming a sputter-deposited reflective film on the tip's surface, a laser beam propagating through the fibre's core was emitted from the sidewall of the fibre. However, as illustrated in Figure 3f, even when the reflective surface was shaped by chemical etching, the emitted laser did not form a visible focus. Therefore, although flow velocity could be measured using this FO-LDV sensor, the measurement volume of the sensor remained undefined. To verify the effect of chemical etching and to clarify the position and size of the measurement volume of this FO-LDV sensor, the emitted laser beam's path and profile were visualised using a laser-induced fluorescence technique in a glycerol solution with a refractive index matched to that of engine oil.

As shown in Figure 6a, a plexiglass tank was filled with a glycerol–water solution containing Rhodamine B (Fujifilm Wako Pure Chemicals, Osaka, Japan, 183-00122; excitation wavelength, 550 nm; fluorescence wavelength, 580 nm) at a concentration of C = 0.5 mg/L. The refractive index of the glycerol–water solution was measured using an Abbe refractometer, and the concentration of the solution was adjusted to match the refractive index of the lubricating oil used in the engine bench test at n = 1.466. The FO-LDV sensor was positioned in the tank such that the emitting laser's path from the fibre was parallel to the tank's bottom. A continuous-wave laser from a laser diode (Neoark, Hachioji, Japan, NEO-100-SG; λ = 533 nm; output power P = 100 mW) was introduced into the fibre and emitted from the FO-LDV sensor. The fluorescence produced where the laser transmitted through the glycerol–water solution was observed with a digital single-lens reflex (SLR) camera (Nikon, Tokyo, Japan, D300) equipped with a long-pass filter (Kanomax, Suita, Japan, HP-570; cut-on wavelength, λ = 570 nm) and recorded on a PC.

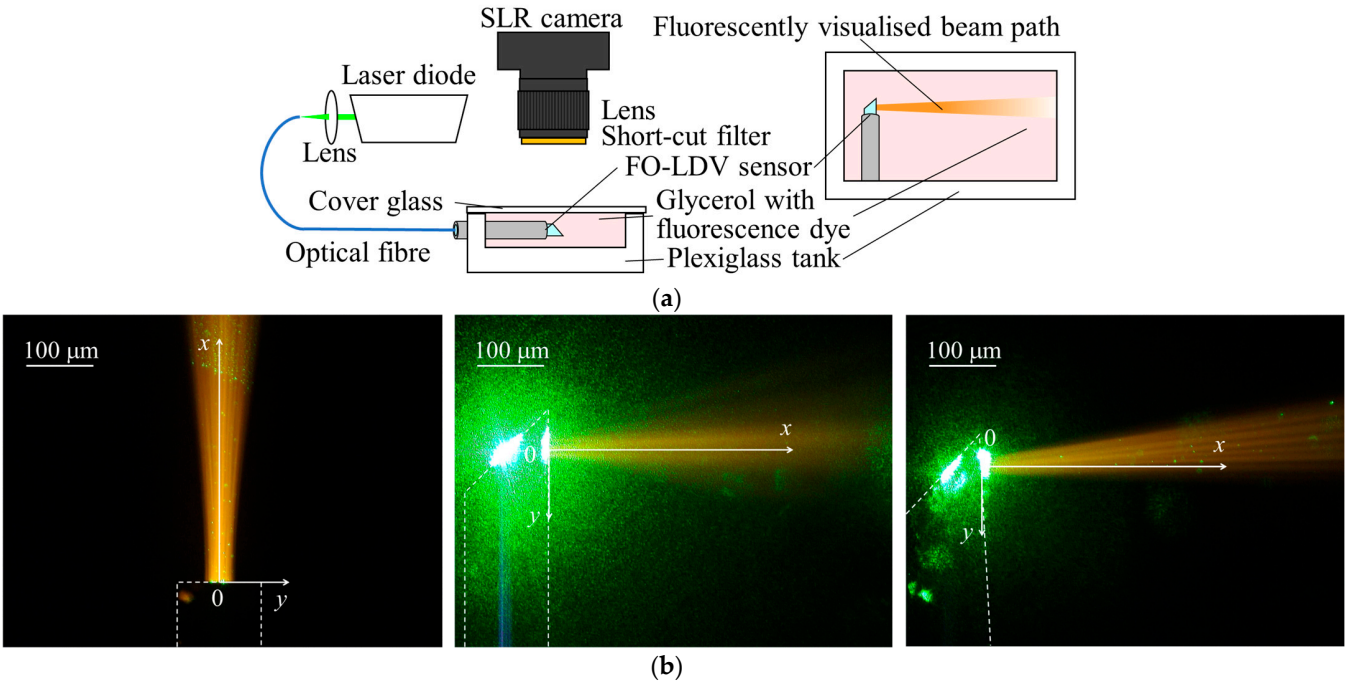

Figure 6. *Cont.*

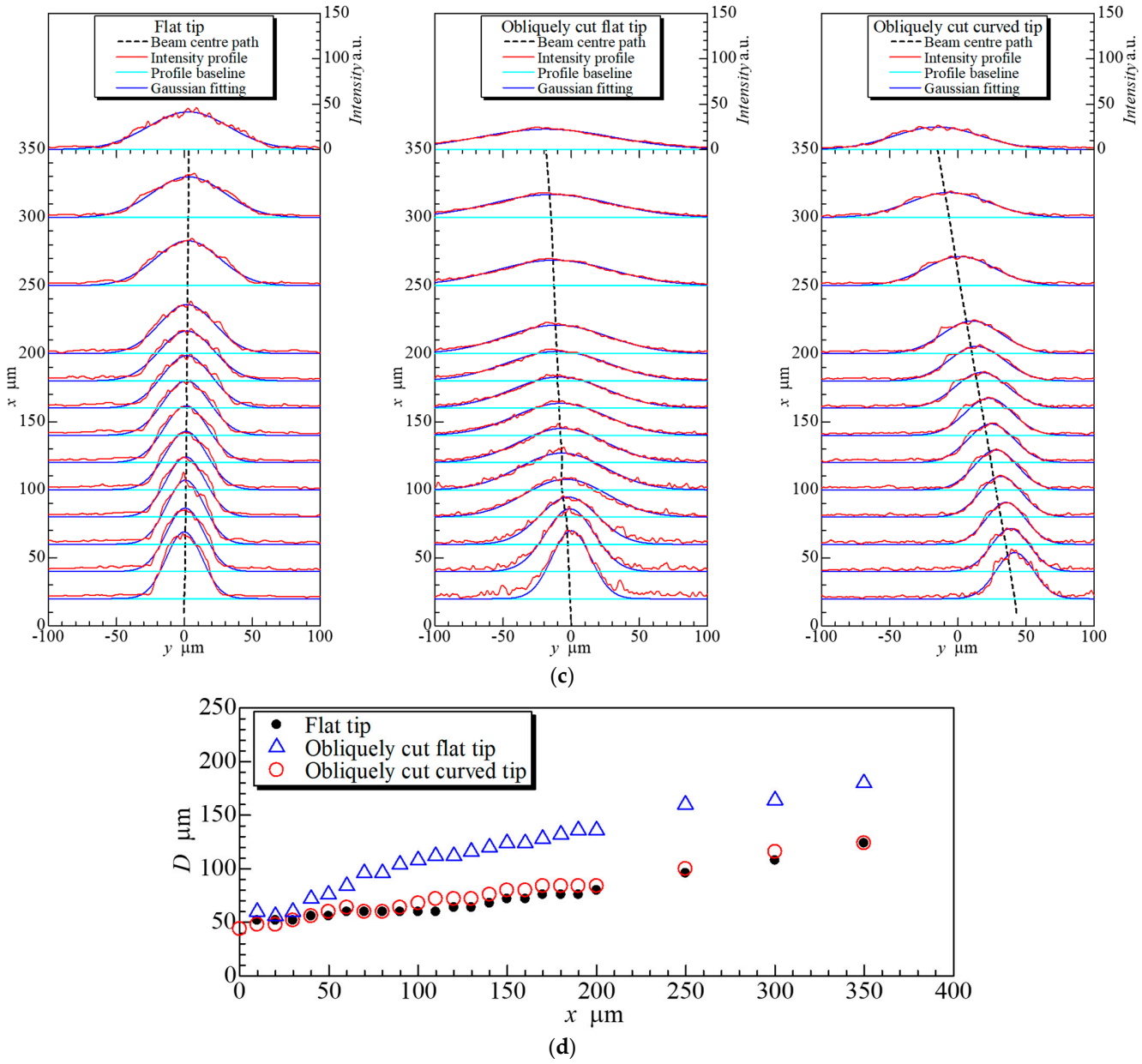

Figure 6. Evaluation of the laser beam emitted from the FO-LDV sensor. (**a**) Outline of the experimental apparatus for observation of the emitting laser's path via the laser-induced fluorescence method. (**b**) Examples of laser-induced fluorescence images by the laser beam emitted from the sensor, recorded without the fluorescence filter. The green light was the source light from the laser, whereas the orange light is the fluorescence. The path of the laser emitted from the normally cut fibre (left). The path of the laser from the obliquely cut fibre with a flat mirror (middle). The path of the laser from the obliquely cut fibre with a curved mirror (right). (**c**) Results of image analysis of the emitted laser beam's profiles, width, and path corresponding to Figure 6b. (**d**) Comparison of the emitted beam's divergence from the FO-LDV sensor. The horizontal axis of the graph exhibits the transmitted distance from the fibre tip, and the vertical axis exhibits the diverged beam's diameter from each fibre tip.

Examples of the visualisation of the path of the transmitted laser emitted from our fabricated FO-LDV sensors are shown in Figure 6b. These colour images were captured without the long-pass filter. These images compared the effects of the chemical etching process with and without a fluoric acid buffer solution prior to the reflective mirror's

deposition. These results demonstrated that the divergence angle of the laser emitted from the fibre varied qualitatively with and without the etching process. To quantitatively evaluate this difference in the laser's path, the images of the fluorescent laser's path (black and white image, 16-bit) using the long-pass filter were analysed using general-purpose image analysis software (ImageJ, NIH, Ver. 1.47). Following median and mean filter processing of the acquired raw images, fluorescence intensity profiles on a line parallel to the central axis of the optical fibre were obtained at intervals of 10 μm from the laser-emitting surface of the fibre. The centre position of the emitted laser beam, the fluorescence intensity at the centre of the beam I_0, and the beam's edges were estimated by Gaussian curve fitting to the fluorescence intensity profiles using the least-squares method. The edges of the beam at each location away from the fibre were defined as the position at which the local fluorescence intensity of the beam was equal to I_0/e^2.

The measured fluorescence intensity profiles of the laser emitted from the FO-LDV sensor, the fitted Gaussian curves, and the penetrating path of the laser beam's centre and edges estimated from the fitting results are depicted in Figure 6c. These findings indicated that a clear focal point was not formed in front of the fibre tip by the FO-LDV sensors. However, the divergence angle of the laser beam's edges was smaller for the chemically etched FO-LDV sensor when compared with the FO-LDV sensor without the etching process. The relationship between the transmission distance x from the fibre and the laser beam's diameter D is illustrated in Figure 6d. As reference data, the paths of the transmitting laser from a normally cut optical fibre tip and a chemically etched FO-LDV sensor with a convex lens-like tip were overlaid on this graph. The results revealed that the width of the laser beam emitted at the fibre tips was approximately 40 μm, with no influence from the shape of the reflection mirror at the tip of the FO-LDV sensors. The width of the laser beam emitted from the non-etched FO-LDV sensor was approximately 140 μm at a distance of 200 μm away from the optical fibre tip. However, the laser beam's width at the same distance was approximately 80 μm using the etched FO-LDV sensor. Additionally, Figure 6b indicates that diffuse reflection occurred at the reflector when using the non-etched FO-LDV sensor. The influence of this diffuse reflection requires clarification and may have influenced the LDV signal's quality due to pedestal noise and the transmitting laser's intensity. These results suggested that the chemical etching process was effective, even if the duration of the etching time was short. However, a focus spot was not observed using the obliquely cut FO-LDV sensor with or without the chemical etching process.

Thereafter, we evaluated the flow measurements during engine bench testing. The volumetric flow rates were calculated by the cross-sectional integration of the velocity profile, as expressed by Equation (3):

$$Q = \int_{-R}^{R} \pi z u(z)\, \mathrm{d}z, \tag{3}$$

where Q is the volumetric flow rate at each location of the velocity measurement, z is the position in the width direction of the oil gallery, and R is the wall position of the oil gallery. The relationship between the calculated volumetric flow rates from the velocity profile and the directly measured flow rate using the Coriolis flowmeter is shown in Table 2. The flow rate at the main gallery was approximately 20% lower than the total lubricant flow rate in the engine system measured with the Coriolis flowmeter.

Table 2. Summary of the validation of the flow velocity measurement in lubricant oil flow during the engine bench test.

Engine speed [rpm]		2000	3000	4000	5000	6000
Flow rate at the oil filter measured by Coriolis flowmeter (L/min)		14.9	16.3	18.0	19.7	20.1
Calculated flow rate by integrating LDV-measured flow velocity profiles (L/min) and the ratio of the difference from the Coriolis flowmeter's measurement (%)	At the main gallery	12.0 (−19.5%)	12.8 (−21.5%)	14.1 (−21.7%)	15.4 (−21.8%)	15.5 (−22.9%)
	At the oil filter port	14.8 (−0.7%)	-	-	-	-

The calculated oil flow rate at the oil filter port had an error of −0.7% relative to the flow rate directly measured with a Coriolis flowmeter. This accuracy was sufficient for measurement of the flow velocity by LDV. However, the calculated flow rates at the main gallery exhibited differences of approximately −20% relative to the Coriolis flowmeter. The oil flow at the oil filter port was diverted into the main gallery in the cylinder block and the balancer shaft of the output shaft of the engine. Thus, the oil flow rate supplied to the balancer shaft could be estimated by the differential of these flow rates. This result indicated that our fabricated FO-LDV sensor was a significantly effective tool for the investigation and optimisation of the lubrication system under high-temperature and high-pressure conditions. This study could measure only the time-averaged flow velocities because a swept spectrum analyser was employed as the signal processing system. However, a previous study [10] could measure the time-resolved flow velocities in unsteady flows using a burst spectrum analyser to analyse a single burst signal from a particle. Therefore, it is expected that the combination of the FO-LDV and the burst spectrum analyser could be used to measure the time-resolved flow velocities in an unsteady opaque flow.

In contrast to typical LDVs, this FO-LDV requires the direct insertion of the sensor's head into the working fluid to measure flow velocity. The insertion of the sensor's head may cause a disturbance of the flow in the flow field. The measurement volume of this FO-LDV was unclear. Computational fluid dynamics (CFD) analysis was conducted on a three-dimensional model with the shape of the FO-LDV sensor to evaluate the disturbance of flow caused by the sensor's insertion. A schematic diagram of the three-dimensional computational fluid domain in the CFD analysis is shown in Figure 7a.

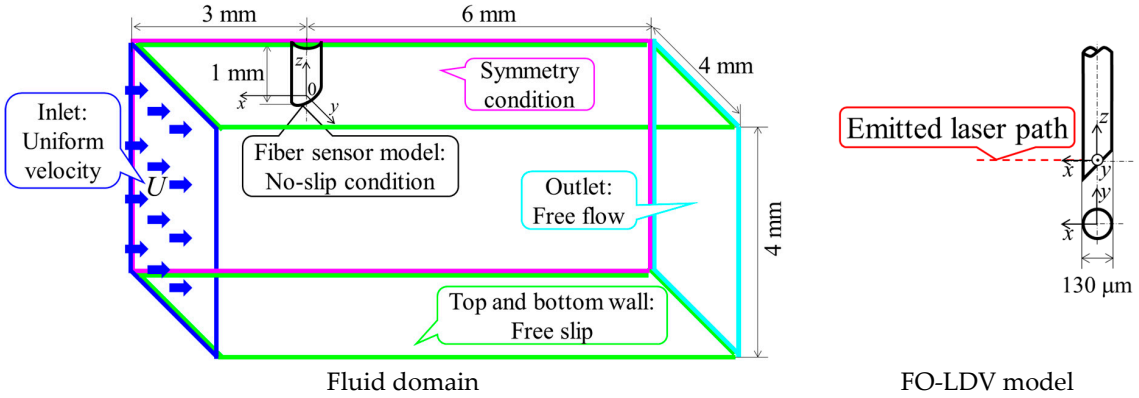

(**a**)

Figure 7. *Cont.*

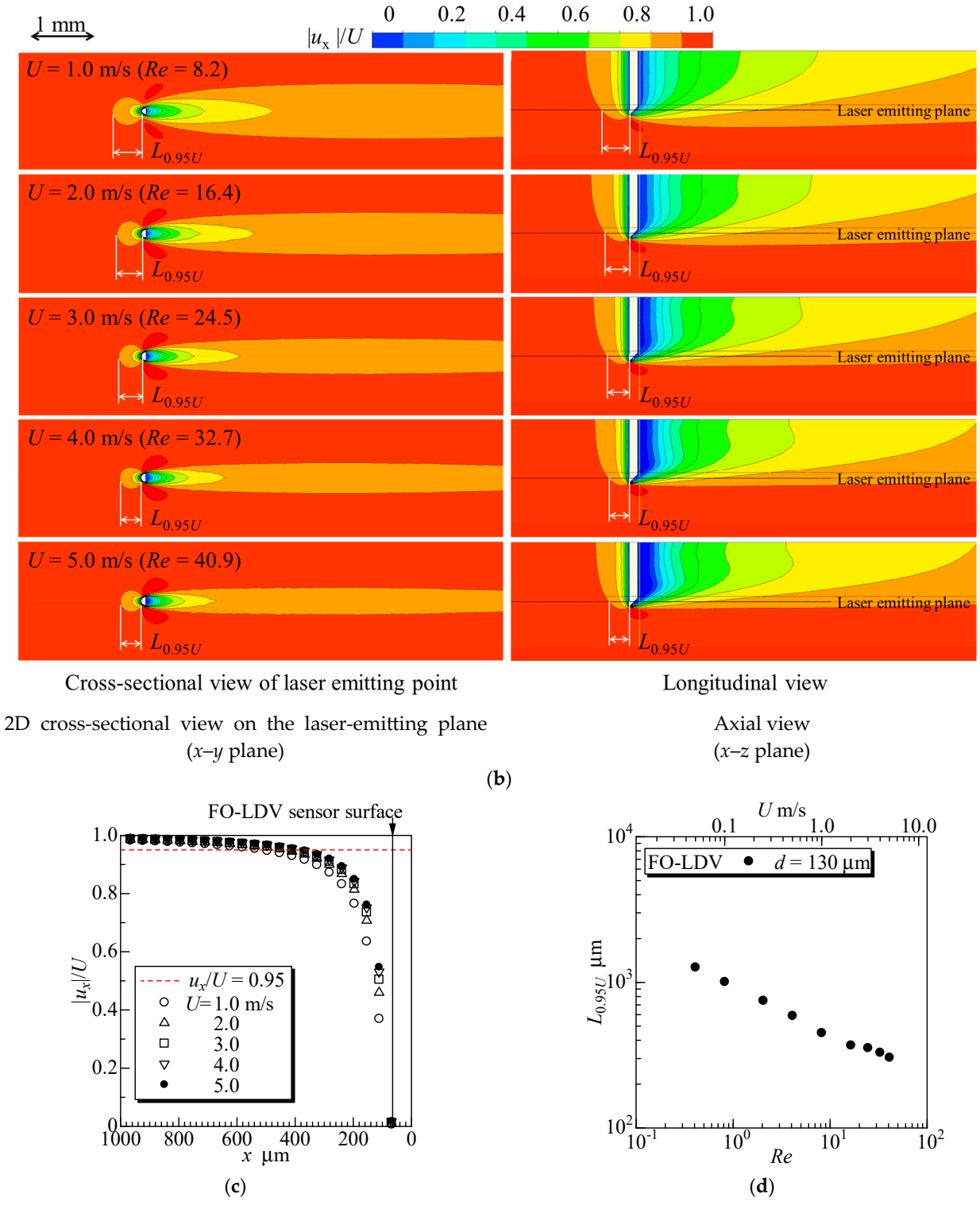

Figure 7. CFD analysis for the flow field around the FO-LDV sensor in a steady and uniform oil flow. (**a**) Fluid domain and boundary conditions for the CFD analysis (left). The model of the FO-LDV sensor (right). (**b**) Examples of the results of CFD analysis. The coloured contour maps reveal the magnitude of the flow velocity in the main flow direction. (**c**) Distribution of the flow speed approaching the FO-LDV sensor on the streamline through the forward stagnation point of the sensor. (**d**) Relationship between the Reynolds number of the flow around the FO-LDV sensor and the thickness of the stagnant layer formed in front of the sensor.

The fluid domain was a rectangular channel with a 4 mm square cross-section and an axial length of 10 mm. The FO-LDV sensor was modelled as an obliquely cut circular cylinder with an outer diameter (d) of 130 μm and an axial length of 1 mm. The model of the FO-LDV sensor was positioned on the upper wall at the centre of the channel's width, 3 mm downstream from the flow inlet. The mechanical properties of the working fluid in the CFD analysis were set to match those of the engine lubricating oil 5W-30, with a dynamic viscosity (μ) of 12.907 mPa·s, a density (ρ) of 813 kg/m^3, and a kinematic viscosity (ν) of 15.874 mm^2/s at an oil temperature of 80 °C during the engine bench test described in Section 3.3. Given that the maximum flow velocity measured by the FO-LDV sensor during the engine bench test was approximately 2.2 m/s, the CFD analysis simulated a scenario in which the model of the FO-LDV sensor was placed in a uniform flow with velocities (U) ranging from 0 to 5 m/s. The Reynolds number of the flow around the FO-LDV sensor was defined by Equation (4), with the FO-LDV sensor's diameter as the representative length and the uniform flow velocity as the representative velocity.

$$Re \equiv \frac{Ud}{\nu} = \frac{\rho Ud}{\mu} \tag{4}$$

Given that the Reynolds number of this flow was below Re = 40.9, if the flow around the FO-LDV sensor was assumed to be two-dimensional, a fixed pair of Föppl vortices would be observed in the cylinder's wake under almost all velocity conditions, and no Kármán vortex shedding would occur [14]. Hence, the CFD area was limited to only half of the fluid domain to balance the computational load and the accuracy of the simulation's results. The boundary conditions of this simulation were set as symmetrical flow at the central longitudinal plane, free slip on the channel's walls, uniform inflow at the inlet, free outflow at the exit, and a no-slip condition on the surface of the model sensor. The fluid domain was meshed into tetrahedral elements using ANSYS Meshing (ANSYS, Ver. 16). Steady-state analyses were performed using ANSYS CFX (ANSYS, Ver. 16) under laminar flow conditions. The simulation results were visualised using ANSYS CFX-Post (ANSYS, Ver. 16).

Figure 7b presents the contour maps of the flow speed around the model of the FO-LDV sensor. These results indicated that a slower flow region, when compared with the uniform flow velocity, was observed in front of the model of the FO-LDV sensor due to the formation of a forward stagnation point. This slower flow region decayed as the Reynolds number increased.

The tolerance for the accuracy of the flow velocity measurements by the FO-LDV sensor was set at 5%, and the distance $L_{0.95}$ was measured from the forward stagnation point on the FO-LDV sensor's surface to the point where the local flow speed was below 95% of the uniform flow velocity on the symmetrical plane. The relationship between the thickness of the stagnant flow region and the main flow velocity is shown in Figure 7c. The results Indicate that the thickness of the stagnant region In front of the FO-LDV sensor was about 1.16 mm at Re = 0.82 and 495 μm at Re = 16.4. Given that the oil flow velocity during the engine bench test was greater than 0.5 m/s, a stagnant region with a thickness of approximately 730 μm was formed in front of the sensor. During the engine bench test, no clear peaks were observed In the spectral waveform when the Doppler frequency was below 0.5 MHz, which corresponded to a flow velocity of 0.11 m/s; thus, a stagnant region with a thickness of approximately 1.2 mm was estimated. Given that the oil flow velocity during the engine bench test was greater than 0.5 m/s and the volumetric flow rate calculated by integrating the velocity profiles was in good agreement with the directly measured flow rate using the Coriolis flowmeter, the measurement volume of the FO-LDV sensor was located in the region approximately 500–1200 μm away from the FO-LDV sensor.

This estimated location of the measurement volume was significantly further away from the FO-LDV sensor than the predicted location of the test volume. To verify the validity of this estimation, we simulated the spectral waveform of the Doppler signal of the

FO-LDV sensor using the CFD results. A conceptual diagram of the optical phenomena occurring on the path of the laser emitted from the FO-LDV sensor, which was scattered by particles in the working fluid until the scattered light returned to the FO-LDV sensor, is shown in Figure 8a. We considered the following five physical phenomena affecting the accuracy of the measurements of flow velocity by FO-LDV.

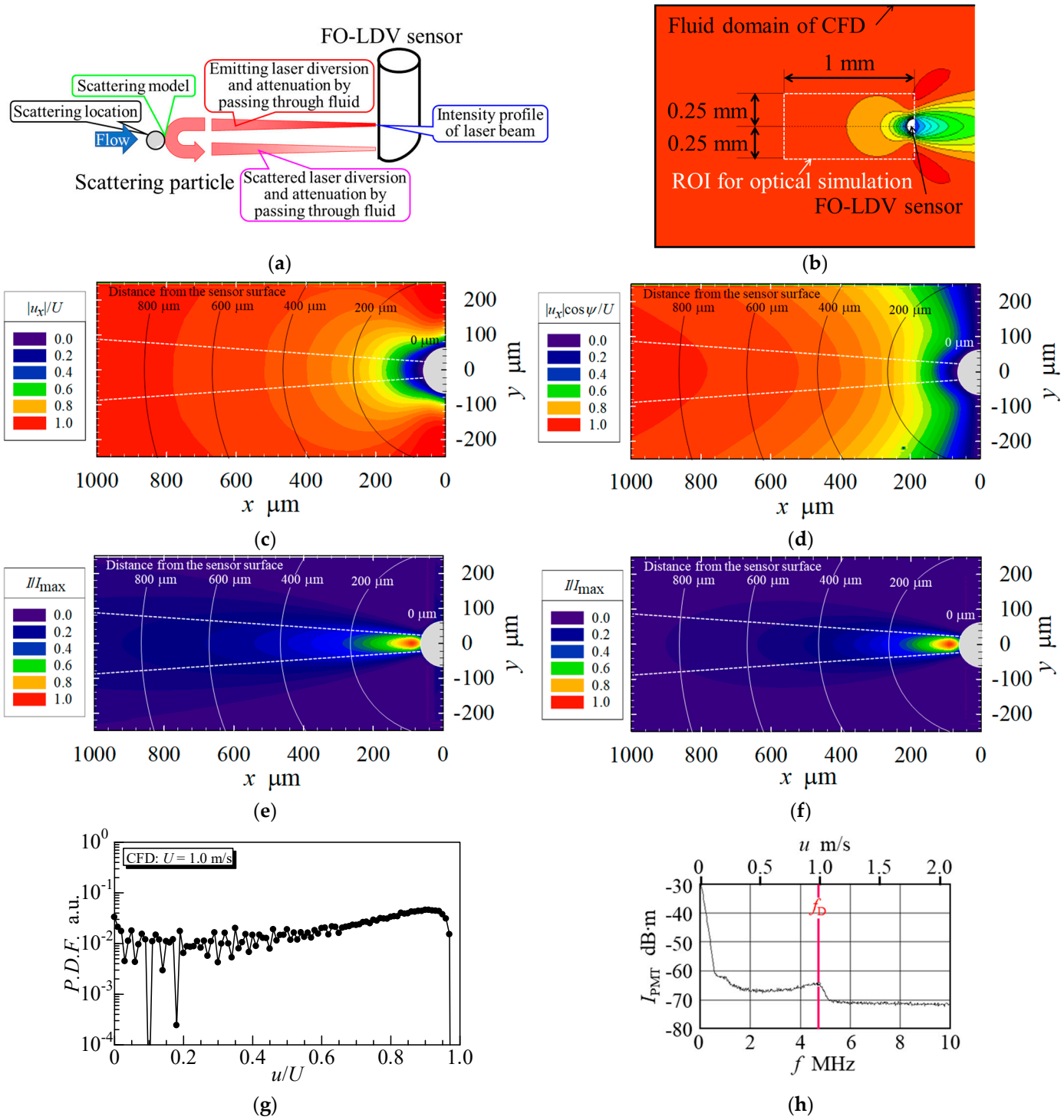

Figure 8. Optical simulation of the FO-LDV measurements was conducted using the results of the CFD analysis for the flow field around the FO-LDV sensor in a steady and uniform oil flow. (**a**) Conceptual diagram of the optical and physical phenomena influencing the accuracy of FO-LDV

measurements. (**b**) Setting of the region of interest (ROI) in the fluid domain of the CFD analysis for the optical simulation. (**c**) Extracted CFD result of the *x*-direction component of the flow velocities in the ROI under U = 1.0 m/s. The coloured contour maps reveal the magnitude of the flow velocity in the main flow direction. (**d**) Distribution of the flow speed approaching the FO-LDV sensor under U = 1.0 m/s. (**e**) Distribution of laser's intensity for a Gaussian beam emitted from the FO-LDV sensor when it reached each position in the ROI. (**f**) Relationship between the backscattered light's intensity due to particles received by the FO-LDV sensor and the particles' position in the ROI. (**g**) Example of the simulated spectral waveform by spatiotemporally integrating the signal/laser intensity-weighted probability of the existence of the flow velocities. (**h**) Example of an experimentally obtained spectral waveform under the same flow condition (U = 1.0 m/s) as the simulation.

1. Differences in the signal intensity were caused by the spatial variation of the intensity of the laser emitted from the FO-LDV sensor.
2. The Doppler frequency was dependent on where the laser was scattered by the suspended particles in the flow field, as the velocity was not uniform in front of the sensor.
3. The suspended particles' localisation in the working fluid caused the maldistribution of the transmitting laser's attenuation and the particles' scattering.
4. The intensity of the scattered laser radiation was dependent on the particles' diameter, the particles' shape, and the scattering angle under the same laser wavelength conditions.
5. Multiple scattering influenced the multiplicity of the Doppler frequency shift and decay of the scattered light's intensity.

First, as demonstrated in Figure 6c, the emitted laser beam travelled straight through the working fluid, and the intensity profiles of the transmitted laser beam exhibited a Gaussian beam profile along the path, with the beam's width being dependent on the distance from the FO-LDV sensor. Therefore, this study assumed that the laser emitted from the sensor was a Gaussian beam with a diameter as expressed by Equation (5):

$$\frac{I(r,L)}{I_0(L)} = \exp\left(\frac{-8r^2}{D^2(L)}\right), \tag{5}$$

where $I_0(L)$ is the intensity of the laser at the centre axis of the beam after travelling a distance L, $I(r, L)$ is the intensity profile of the laser beam, $D(L)$ is the beam's diameter, and r is the radial distance from the centre axis of the beam. It was assumed that the laser beam travelled through the working fluid with a constant divergence angle. Thus, the relationship between the beam's diameter and the laser's travelling distance was modelled as Equation (6)

$$\frac{D(L)}{D_0} = 1 + \frac{2\tan\frac{\phi}{2}}{D_0}L \approx 1 + \phi\frac{L}{D_0}, \tag{6}$$

where D_0 is the diameter of the laser beam at the start of its travel from the FO-LDV sensor, $D(L)$ is the diameter of the laser beam after travelling a distance L, and ϕ is the divergence angle of the laser beam from the FO-LDV sensor. If the divergence angle is sufficiently small, the above approximate equation can be utilised. The centre axis of the Gaussian beam profile travelled directly ahead of the FO-LDV sensor. Additionally, the laser's intensity was attenuated through the opaque working fluid due to the absorption and scattering of light. The attenuation of the transmitted laser's intensity was modelled as obeying the Beer–Lambert law, as expressed by Equation (7):

$$\frac{I_0(L)}{I_0(L=0)} = \exp(-\alpha L), \tag{7}$$

where I_0 (L = 0) is the intensity of the laser at the start of the travel of the beam's centre, $I_0(L)$ is the intensity of the light detected after travelling a distance L, and α is the attenuation

constant of the working fluid. The attenuation constant was dependent on the particles' concentration. However, as depicted in Figure 2c, the concentration of MoS_2 in the engine oil during the engine bench test was considerably high, and the particle size was small. It cannot be assumed that the MoS_2 particles were localised at a specific location in the working fluid. In this study, we assumed that the particles in the working fluid were homogeneously dispersed with a uniform diameter and moved with the local flow speed without sinking or slipping. Therefore, the attenuation constant remained constant without varying with the distance from the FO-LDV sensor.

Second, the Doppler frequency shift due to the Doppler effect of the flowing particles in the working fluid was modelled using Equation (1). Given that the homogeneous dispersion of the particles suspended in the working fluid caused light scattering throughout the transmitted path of the laser beam emitted from the sensor, the magnitude of the Doppler frequency shift was dependent on where the laser was scattered. Additionally, as the emitted laser beam had a diameter and a divergence angle, the angle ψ between the local flow velocity vector and the optical path to the transmitting optic object detector varied at each scattering location. Hence, the Doppler effect was modelled as expressed by Equation (8):

$$f_D(x,y) \simeq \frac{2n}{\lambda_0}|u(x,y)\cos\psi(x,y)|, \tag{8}$$

where x and y are the position coordinates of particle scattering, $u(x, y)$ is the local flow speed at the location of particle scattering, and ψ is the angle between the local flow speed parallel to the main flow and the direction of the scattering light's path. Therefore, the FO-LDV system measured the probability of the existence of the flow velocity in the emitted laser beam.

Third and fourth, the size and dispersion of the MoS_2 particles in the working fluid were assumed to be homogeneous. Thus, scattering of the laser by particles occurred with the same probability per unit of time in the laser beam's path, and the intensity of the scattered light was not dependent on the particle size. However, the size and shape of the particles influenced the distribution of the scattered laser's intensity. Given that the diameter of the suspended MoS_2 particles was 1.69 µm, Mie scattering was likely, given the particle size. In [15], given that it was reported that the particle shape of MoS_2 is not spherical, the validity of employing Mie theory was unclear. In Mie scattering, it is common knowledge that the light intensity of the forward-scattered light (the scattering angle is 0°) is the highest, whereas the backscattered light (the scattering angle is 180°) is lower by a factor of 10^{-3}–10^{-5}. At other scattering angles, the intensity of the scattered laser's radiation is significantly dependent on the scattering angle. Given the small optical aperture of the FO-LDV sensor and the narrow divergence of the emitted laser beam from the FO-LD sensor, it was estimated that the FO-LDV sensor could only receive backscattered light and not light scattered at other angles. Therefore, in this study, as modelled, the sensor could only receive scattered laser light from a particle if the transmission path of the outgoing laser from the sensor to the scattered particle and the transmission path of the scattered laser from the particle to the sensor were coincident. Given that the simulation considered backscattered light, the ratio of the scattered light's intensity I_{sc} to the incident light's intensity I_{in} was modelled as a constant ζ, as shown in Equation (9):

$$I_{sc}(x,y) = \zeta I_{in}(x,y). \tag{9}$$

During the backward laser transmission, attenuation of the laser's intensity was considered, as described by the Beer–Lambert law in Equation (7).

Fifth, scattered light with scattering angles other than 0° and 180° could be detected by the sensor through multiple scattering. Given that the receivable range of the sensor was considerably narrow, the multiply scattered light may be significantly attenuated before reaching the sensor's aperture through numerous scatterings. If backscattered light from a particle reached the FO-LDV sensor without additional scattering by another particle, its

intensity was influenced only by the attenuation of transmission. The intensity of multiply scattered light was significantly weaker than that of singly scattered light. Thus, multiple scattering was neglected in this study.

The factors mentioned above influenced the Doppler signal intensity of the laser received by the FO-LDV sensor. The scattering laser intensity from a scattering particle was estimated by combining Equations (5)–(7) and (9), as expressed by Equation (10):

$$I_{DS}(x,y) = I_0(L=0)\zeta \exp\left(\frac{-8r^2}{(D_0+\phi L)^2} - 2\alpha L\right), \tag{10}$$

where I_{DS} is the Doppler signal intensity due to each scattering particle. In experiments, increasing the applied voltage of the photomultiplier tube could enhance the amplification factor. However, the amplification factor was assumed to be not influenced by the frequency and was neglected in this simulation. Therefore, the frequency spectrum waveform for the CFD-analysed flow field was obtained by spatiotemporally superimposing the relationship between the flow velocity (i.e., the Doppler frequency) and the signal intensity (that is, scattered light intensity), as expressed by Equation (11):

$$P.D.F.(u \propto f_D) = \iint_{ROI} I_{DS}\mathrm{d}x\mathrm{d}y, \tag{11}$$

where *P.D.F.* represents the simulated spectral waveform. Although the spectral waveform was inherently influenced by the integration time, this effect was neglected in this simulation because it was assumed that the scattered particles were uniformly dispersed in the working fluid and that the occurrence of light scattering per unit time at any location was the same.

We attempted to detect the Doppler frequency of the flow from the simulated spectral waveforms to estimate the measurement volume of the FO-LDV sensor. The simulation conditions were based on the abovementioned experimental results, with the attenuation constant of the Beer–Lambert law in the lubricant oil with MoS_2 particles set to α = 0.25 mm^{-1} based on actual measurements of the oil used in the engine bench test. The laser beam emitted from the FO-LDV sensor was modelled as a Gaussian beam with a diameter of D_0 = 40 μm and with the beam's divergence angle set to 4.4°. In this simulation, it was assumed that all the laser light received by the FO-LDV sensor from the scattered particles was only backscattered light. Hence, all receiving paths of the scattered laser were perpendicular to the surface of the FO-LDV sensor, which had a circular cross-section. Therefore, the influence of the transmission attenuation on the light intensity across the interface between the working fluid and the FO-LDV sensor was assumed to be negligible in this simulation.

As shown in Figure 8b, a region of interest (ROI) for optical simulation was established with a length of 1 mm upstream from the centre of the sensor and a half-width of 0.25 mm on each side perpendicular to the main flow from the sensor's centre. This ROI was divided by a 5 μm square orthogonal grid. The flow speeds at each grid point were linearly interpolated from the CFD results, as depicted in Figure 8c. The white dashed line in the graph represents the width of the Gaussian beam emitted from the sensor, and the black solid line of concentric circles indicates the distance from the surface of the FO-LDV sensor within the ROI. Considering the difference between the scattering angle and the main flow direction, the distribution of the approaching flow speed was calculated as shown in Figure 8d. The laser intensity achieved at a position in the ROI decayed exponentially with respect to the transmitting distance, as illustrated in Figure 8e. Therefore, the intensity of the emitted light was stronger closer to the FO-LDV sensor within the ROI, and the intensity was higher along the central axis of the beam's path due to the influence of the Gaussian beam. The laser reaching a scattering particle was backscattered at each location and transmitted the same distance through the working fluid, and thereafter decaying

and resulting in a decrease in the intensity of the laser received by the FO-LDV sensor, as expressed by Figure 8f.

The spectral waveforms of the scattered light received by the FO-LDV sensor were calculated by integrating the laser intensities for the same approach speed of the particle. An example of the simulation's results is shown in Figure 8g, and an experimentally acquired spectral waveform during the engine bench test under the same flow condition is shown in Figure 8h. This result indicated that these two frequency spectrum waveforms were significantly similar, although differences could be observed in the pedestal noise, which represented the DC component. The flow velocity measured from this simulated spectral waveform was u = 0.97 m/s. In a comparison of Figure 8c,d, the region of flow with the peak intensity of the spectral waveform of flow velocity was located more than 800 μm away from the FO-LDV sensor, and the laser transmitted through the region had a width of 200 μm. It was suggested that the measurement volume of the proposed FO-LDV sensor was estimated to be centred at a distance of approximately 900 μm from the sensor, with a measurement volume of 200 μm in length in the flow direction and 200 μm in width perpendicular to the flow.

Given that this simulation did not consider the distribution of flow velocities along the longitudinal axis of the FO-LDV sensor, the thickness of the measurement volume of the sensor could not be accurately estimated. However, the CFD analysis results, as shown in Figure 7b, indicated that the flow at a distance of 1 mm upstream from the sensor did not exhibit a broad distribution of velocity in the long-axis direction of the sensor, thus suggesting that the thickness of the measurement volume was estimated to be approximately the same as the width. The results suggest that, with right-angle insertion of the FO-LDV sensor, the light emitted from the sensor did not require the formation of a focal point and should be maximally collimated.

5. Conclusions

This article presents a novel FO-LDV sensor and its performance. With reference to the available literature, this is the first direct measurement of the velocity profile of lubricating oil in a cylinder block during engine bench testing. The accuracy of the FO-LDV measurements was compared with the volumetric flow rate obtained by integration of the cross-sectional area of the flow velocity profile and that measured using a Coriolis flowmeter, and the difference was within 1%. The flow rate through the main gallery, which was diverted after passing through the oil filter section, was found to be 20–22% lower than that in the oil filter section, thus accounting for the difference in the flow rate supplied to the balancer shaft. With reference to the available literature, this represents the first direct measurement of the diversion of the flow rate in lubricating oil flow. Furthermore, by combining CFD analysis and computer simulations of the laser's attenuation and particle scattering in the transmission of light through a working fluid, we estimated the spectral waveform of the FO-LDV sensor. It was suggested that the FO-LDV sensor had a measurement volume of 200 microns in length and 200 microns in width at a distance of 900–1000 microns forward from the sensor. The FO-LDV sensor was able to provide accurate measurements of the velocity profile, even in opaque, high-temperature, and high-pressure fluids. In future work, the FO-LDV sensor will be combined with a burst spectrum analyser to measure time-resolved flow velocities in lubricating oil flow.

Author Contributions: Conceptualisation, T.T., S.K. and K.O.; methodology, T.T., S.K., T.M., T.F. and H.Y; software, T.T; validation, T.T., S.K., T.M., T.F. and H.Y.; data curation, T.T. and S.K.; writing—original draft preparation, T.T.; writing—review and editing, T.T.; visualisation, T.T. and S.K.; supervision, T.T., S.K. and K.O.; project administration, T.T., S.K., and K.O.; funding acquisition, T.T. and K.O. All authors have read and agreed to the published version of the manuscript.

Funding: This research was funded by the Japan Science and Technology Agency (JST), A-STEP Grant Number AS2111345B.

Institutional Review Board Statement: Not applicable.

Informed Consent Statement: Not applicable.

Data Availability Statement: The data are not publicly available because they contain information that could compromise the privacy of the research participants.

Acknowledgments: We thank the staff of Out-Sourcing Central Inc. for their assistance with the engine bench tests.

Conflicts of Interest: The authors declare no conflicts of interest.

References

1. Tanaka, T.; Benedek, G.B. Measurement of the velocity of blood flow (in vivo) using a fiber optic catheter and optical mixing spectroscopy. *Appl. Opt.* **1975**, *14*, 189–196. [CrossRef] [PubMed]
2. Kajiya, F.; Hoki, N.; Tomonaga, G.; Nishihara, H. A laser-Doppler-velocimeter using an optical fiber and its application to local velocity measurement in the coronary artery. *Experientia* **1981**, *37*, 1171–1173. [CrossRef] [PubMed]
3. Nishihara, H.; Koyama, J.; Hoki, N.; Kajiya, F.; Hironaga, M.; Kano, M. Optical-fiber laser Doppler velocimeter for high-resolution measurement of pulsatile blood flows. *Appl. Opt.* **1982**, *21*, 1785–1790. [CrossRef] [PubMed]
4. Kajiya, F.; Mito, K.; Ogasawara, Y.; Tsujioka, K.; Tomonaga, G.; Nishihara, H.; Hironaga, M.; Kano, M. Laser Doppler Blood Flow Velocimeter with an Optical Fiber and Its Application to Detailed Measurements of the Coronary Blood Flow Velocities. In Proceedings of the SPIE 0494 Novel Optical Fiber Techniques for Medical Applications, San Diego, CA, USA, 24 October 1984. [CrossRef]
5. Kajiya, F.; Tsujioka, K.; Goto, M.; Wada, Y.; Tadaoka, S.; Nakai, M.; Hiramatsu, O.; Ogasawara, Y.; Mito, K.; Hoki, N.; et al. Evaluation of phasic blood flow velocity in the great cardiac vein by a laser Doppler method. *Heart Vessel.* **1985**, *1*, 16–23. [CrossRef] [PubMed]
6. Mito, K.; Ogasawara, Y.; Hiramatsu, O.; Tsujioka, K.; Kajiya, F. A laser Doppler catheter for monitoring both phasic and mean coronary vein flow. *Heart Vessel.* **1990**, *6*, 1–8. [CrossRef] [PubMed]
7. Kajiya, F. Characteristics and possible origins of blood velocity waveforms of the epicardial and intramyocardial coronary circulation in the ventricles and the atria. In *Coronary Circulation in Physiological and Pathophysiological States*; Nakamura, M., Vanhoutte, P.M., Eds.; Springer: Tokyo, Japan, 1991; pp. 1–19. [CrossRef]
8. Ohba, K.; Fujiwara, N. Development of fiber optic laser Doppler velocimeter for measurement of local blood velocity. In Proceedings of the SPIE2052 Fifth International Conference on Laser Anemometry: Advances and Applications, Koningshof, Veldhoven, The Netherlands, 6 August 1993. [CrossRef]
9. Tajikawa, T.; Takeshige, M.; Ishihara, W.; Kohri, S.; Ohba, K. Development of miniaturized fiber-optic laser Doppler velocimetry sensor for measurement of local blood velocity (fabrication method for convex or concave lens-like fiber tip and the characteristics of sensor optical system). *J. Fluid Sci.Technol.* **2009**, *4*, 62–74. [CrossRef]
10. Kohri, S.; Tajikawa, T.; Ohba, K. Development of a miniaturized fiber-optic LDV sensor for local blood velocity measurement. *Biomed. Eng. Res.* **2013**, *2*, 131–138. [CrossRef]
11. Cai, H.; Larsson, S.E.; Oberg, P.A. Single fiber laser-Doppler flowmetry—Dependence on wavelength and tip optics. *J. Biomed. Opt.* **1998**, *3*, 34–339. [CrossRef] [PubMed]
12. Scalise, L.; Steenbergen, W.; De Mul, F. Self-mixing feedback in a laser diode for intra-arterial optical blood velocimetry. *Appl. Opt.* **2001**, *40*, 4608–4615. [CrossRef] [PubMed]
13. Okada, A.; Sholes, K.; Sotono, Y.; Tajikawa, T.; Kohri, S.; Ohba, K. Application of Fiber LDV to the Measurement of Engine Oil Flow Rate. In Proceedings of the Society of Automotive Engineers of Japan, Autumn Congress 2012, Osaka, Japan, 3–5 October 2012; Available online: https://tech.jsae.or.jp/paperinfo/ja/content/p2012141.01/ (accessed on 15 March 2024).
14. Lienhard, J.H. *Synopsis of Lift, Drag, and Vortex Frequency Data for Rigid Circular Cylinders*; Bulletin 300; Washington State University: Pullman, WA, USA, 1966; pp. 1–32.
15. Molybdenum Disulfide (MoS2) Powder. Available online: https://www.acsmaterial.com/molybdenum-disulfide-mos2-powder.html (accessed on 12 June 2024).